Diffusion-assisted selective dynamical recoupling: A new approach to measure background gradients in magnetic resonance

Gonzalo A. Álvarez, Noam Shemesh, and Lucio Frydman

Citation: The Journal of Chemical Physics **140**, 084205 (2014); doi: 10.1063/1.4865335
View online: http://dx.doi.org/10.1063/1.4865335
View Table of Contents: http://scitation.aip.org/content/aip/journal/jcp/140/8?ver=pdfcov
Published by the AIP Publishing

Diffusion-assisted selective dynamical recoupling: A new approach to measure background gradients in magnetic resonance

Gonzalo A. Álvarez, Noam Shemesh, and Lucio Frydman[a)]
Department of Chemical Physics, Weizmann Institute of Science, Rehovot 76100, Israel

(Received 16 October 2013; accepted 26 January 2014; published online 27 February 2014)

Dynamical decoupling, a generalization of the original NMR spin-echo sequence, is becoming increasingly relevant as a tool for reducing decoherence in quantum systems. Such sequences apply non-equidistant refocusing pulses for optimizing the coupling between systems, and environmental fluctuations characterized by a given noise spectrum. One such sequence, dubbed Selective Dynamical Recoupling (SDR) [P. E. S. Smith, G. Bensky, G. A. Álvarez, G. Kurizki, and L. Frydman, Proc. Natl. Acad. Sci. **109**, 5958 (2012)], allows one to coherently reintroduce diffusion decoherence effects driven by fluctuations arising from restricted molecular diffusion [G. A. Álvarez, N. Shemesh, and L. Frydman, Phys. Rev. Lett. **111**, 080404 (2013)]. The fully-refocused, constant-time, and constant-number-of-pulses nature of SDR also allows one to filter out "intrinsic" T_1 and T_2 weightings, as well as pulse errors acting as additional sources of decoherence. This article explores such features when the fluctuations are now driven by unrestricted molecular diffusion. In particular, we show that diffusion-driven SDR can be exploited to investigate the decoherence arising from the frequency fluctuations imposed by internal gradients. As a result, SDR presents a unique way of probing and characterizing these internal magnetic fields, given an *a priori* known free diffusion coefficient. This has important implications in studies of structured systems, including porous media and live tissues, where the internal gradients may serve as fingerprints for the system's composition or structure. The principles of this method, along with full analytical solutions for the unrestricted diffusion-driven modulation of the SDR signal, are presented. The potential of this approach is demonstrated with the generation of a novel source of MRI contrast, based on the background gradients active in an *ex vivo* mouse brain. Additional features and limitations of this new method are discussed. © *2014 AIP Publishing LLC*. [http://dx.doi.org/10.1063/1.4865335]

I. INTRODUCTION

Even when subject to a strong, uniform external field, nuclear spins experience fluctuations in their nuclear magnetic resonance (NMR) frequencies. These will arise from the orientation- and the position-dependencies that characterize the NMR interactions.[1] In heterogeneous systems in particular, susceptibility differences between various matrices and interfaces give rise to (often complicated) spatially-varying magnetic field patterns $\Delta\mathbf{B_0}(\mathbf{r})$.[2–5] Spins residing in these interface locations – which may span length-scales ranging from nanometers in porous systems to macroscopic lengths – will experience a range of frequency offsets $\Delta\nu = \gamma\Delta B_0$. These offsets will appear as an effective line broadening in the NMR spectrum, shortening the transverse dephasing rate of the ensemble. If these susceptibility-driven offset distributions[6] do not have a zero average, the NMR signals may also experience frequency shifts.[7] While a complication in high-resolution NMR, such susceptibility-induced effects have proven remarkably useful for NMR imaging (MRI). In MRI of the Central-Nervous-System, for example, phase maps can generate unique, susceptibility-weighted-imaging contrasts.[7–9] Furthermore, time-dependent T_2^* contrasts form the basis of functional MRI, which reflects susceptibility-driven variations between oxygenated and oxygen-deprived blood.[10] Recently, it has been further demonstrated that the susceptibility tensor can be characterized by a rotation of the specimen with respect to $\mathbf{B_0}$,[11] yielding remarkably detailed information on local magnetic field anisotropies, and providing a new means for inferring microstructural orientations.[12,13] T_2^* is also emerging as an orientation-dependent marker,[14,15] suggesting its potential usefulness for characterizing the composition[16] and/or microstructure[12,17] of complex systems.

Despite all this clear potential, the detection of the aforementioned effects may be hampered by inherent complications arising from global static-field distortions; macroscopic artifacts that are unrelated to the interfacial (and usually microscopic-level) effects being sought. Applying refocusing π-pulses can compensate for the evolutions incurred from these static $\mathbf{B_0}$ distortions, but at the expense of the information on the desired susceptibility-induced effects – which will also be refocused upon applying π-pulses. Spatially-varying local magnetic fields, often termed "background gradients,"[18] can still be measured if aided by molecular diffusion effects.[19,20] Spins diffusing in susceptibility-driven internal gradients will accumulate phases that cannot be refocused by the application of π-pulses, since a phase evolved at a position $\mathbf{r_1}$ will not necessarily be refocused by a time-reversed evolution at another position $\mathbf{r_2}$. In NMR/MRI, such

a)Electronic mail: lucio.frydman@weizmann.ac.il

effects are exploited for extracting diffusion coefficients, usually with the aid of external diffusion-sensitizing gradients. Internal gradients, however, will also interact with these external fields, producing cross-terms that may hamper accurate measurements of diffusion-derived phenomena.[18] Numerous methods have been proposed and implemented for counteracting these background gradients effects.[3,18,21–28] Conversely, Cho *et al.*[29] have recently shown that internal field distributions can be obtained from the cross-terms between the applied diffusion gradients and the internal fields. Han *et al.* demonstrated how this concept can be used further to derive orientations of anisotropic systems.[30] Diffusion measurements under the sole influence of the internal gradients are also feasible; they are the basis of the Decay due to Diffusion in Internal Fields (DDIF) approach,[3,20,31–33] which determines rock microstructures utilizing the internal gradients as the diffusion-sensitizing "apparatus." Other studies explored diffusion in the presence of a constant background gradient modulated by a different number of pulses or by different evolution times.[19,34] Still, as these methods are not applied in a constant-time and constant number of pulses fashion, they are prone to other decoherence sources such as T_2, pulse artifacts or T_1 losses.

In the present article, we propose an alternative methodology for measuring the internal gradients directly: in a constant-time fashion, using a constant number of π-pulses, and without introducing external diffusion-sensitizing gradients. The approach is based on the recently introduced Selective-Dynamical-Recoupling (SDR) concept,[35,36] which entails varying the delay distributions of N refocusing π-pulses applied over a constant evolution time. SDR has been recently shown sensitive to diffusion-driven decohering effects when a constant external gradient was applied, yielding accurate compartment sizes when spins undergo restricted diffusion.[36,37] Here, we extend these concepts by assuming that susceptibility-driven background gradients are the only source of (unrestricted) diffusion-driven decoherence; thus, characterizations of internal gradients in heterogeneous systems are made possible, with the aid of the free diffusion coefficients that can be measured in separate experiments.

We set forth in Sec. II, the theory for SDR under the influence of a background gradient and show how SDR can quantify these background gradients as aided by unrestricted diffusion. An application of SDR in MRI, aimed at detecting internal gradients in *ex vivo* mouse brains, is presented in Sec. IV (experimental setup details are given in Sec. III). Section V concludes with a discussion on potential extensions of these concepts.

II. SELECTIVE DYNAMICAL RECOUPLING OF BACKGROUND GRADIENTS ASSISTED BY FREE DIFFUSION

We consider spins-1/2 $\hat{S}$ that are solely coupled to a longitudinal magnetic field $\mathbf{B_0}$ and that are part of a fluid immersed in a heterogeneous structure. Two sources of static magnetic field variations may influence these spins: (1) (unwanted) effects arising from inhomogenities in the external magnetic field, (2) (sought) variations arising from inhomogenities induced by susceptibility differences between the immersed fluid and the structure's interface. As a result of these variations, diffusing spins will experience fluctuations in their felt magnetic field. In the usual NMR resonant rotating frame,[38] the relevant Hamiltonian is $\widehat{\mathcal{H}}_{SE}(t) = \omega_{SE}(t)\hat{S}_z$, where $\omega_{SE}(t)$ is a fluctuating frequency (noise) originated by the random motions. Under the assumption that diffusing spins will acquire a random phase $\phi_i(t)$ exhibiting a Gaussian distribution,[39] the total signal arising from the spin ensemble at an evolution time TE will be: $M(TE) = \sum_i e^{-i\phi_{i,0}(TE) - \frac{1}{2}[\langle\phi_i^2(TE)\rangle - \phi_{i,0}^2(TE)]}$. Here, the average value of the random phase, $\phi_{i,0}(t) = \langle\phi(t)\rangle$, depends on the position of the spin.

Normally, the decay of this magnetization will be driven by inhomogenities of the external magnetic field.[40] These effects can be reduced by applying refocusing pulses. We consider thus the application of a spin-echo sequence that periodically reverses the spins' phases, and hence reduces the effects of static external magnetic field inhomogenities[41–43] We focus in particular on the SDR scheme[35,36] (Fig. 1), a sequence which can be divided into two parts: a CPMG modulation involving $N-1$ pulses[42,43] with a delay x, and a Hahn-echo refocusing period[41] of duration y. Whereas without these pulses the average evolution of each spin will depend on its position in the sample, SDR's fully-refocused nature makes the average phase $\phi_{i,0}(TE) = 0$. This results in a signal $M(TE) = e^{-\frac{1}{2}\langle\phi^2(TE)\rangle}$; a decay that can be quantified by the exponentials argument[44,45]

$$\frac{1}{2}\langle\phi^2(TE)\rangle = \frac{1}{2}\int_{-\infty}^{\infty} d\omega S(\omega)|F(\omega, TE)|^2. \qquad (1)$$

In this equation, $F(\omega, TE)$ is a filter function, given by the Fourier transform of the modulation function $\sqrt{2\pi}\, f_N(t', TE)$ that switches between ± 1 at the position of every pulse (Fig. 1(b)).[46–49] $S(\omega)$ is the spectral density of the precession frequency fluctuation, given by the Fourier transform of the auto-correlation function $g(\tau) = \langle\Delta\omega_{SE}(t)\Delta\omega_{SE}(t+\tau)\rangle$, where $\Delta\omega_{SE}(t)$ is the instantaneous frequency deviation from the average value at time t. This $\Delta\omega_{SE}(t) = \gamma\langle G\rangle[r(t) - \langle r(t)\rangle]$ reflects in turn the mean average gradient $\langle G\rangle$ felt by the randomly walking spin, as well as the

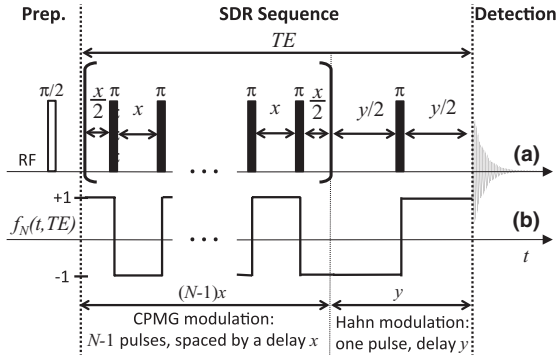

FIG. 1. Selective dynamical recoupling NMR sequence for probing a diffusion spectrum and background gradients. (a) Sequence of N RF π pulses applied to the nuclear spins during the total evolution time TE, incorporating a CPMG sequence with pulses spaced by x and a Hahn sequence of echo time y. (b) Modulating function $f_N(t', TE)$ of the resulting sequence.

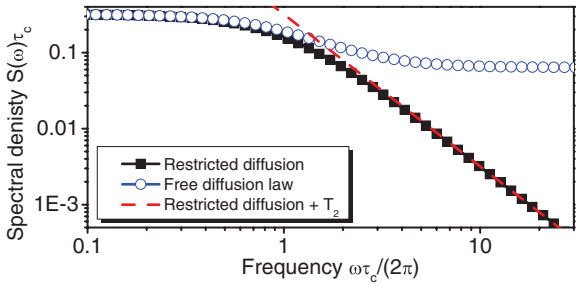

FIG. 2. Spectral density of the frequency fluctuations due to diffusion $S(\omega) = \frac{\Delta\omega_{SE}^2 \tau_c}{(1+\omega^2\tau_c^2)\pi}$ (black squares). The dashed line shows the free diffusion regime given by the power law tail $\propto\omega^{-2}$ for frequencies larger than the inverse of the fluctuation correlation time $1/\tau_c$. Empty circles show the change in this spectrum upon considering the addition of an effective T_2-like decay assumed constant ($T_2 = 5\tau_c$), whose spectral density is independent of the frequency.

displacement fluctuation $r(t) - \langle r(t)\rangle$ along the magnetic field gradient direction.[50] Assuming that diffusion takes place under the Gaussian random-phase approximation[50] this autocorrelation will be characterized by an exponential decay: $g(\tau) = \Delta\omega_{SE}^2 \exp\{-|\tau|/\tau_c\}$, where $\Delta\omega_{SE}^2 = \langle\Delta\omega_{SE}^2(0)\rangle$ is a mean square frequency and τ_c is the fluctuation's correlation time. Plausible spectral density functions associated with different fluctuating models are plotted in Fig. 2. Notice that since these fluctuations are wholly ascribed to translational motions, $S(\omega)$ will be proportional to the molecular diffusion spectral density $D(\omega)$: $D(\omega) = \omega^2 S(\omega)/(\langle G\rangle^2\gamma^2)$.[51,52] It then follows that $\langle\Delta\omega_{SE}^2\rangle = \gamma^2\langle G\rangle^2 D_0\tau_c = \gamma^2\langle G\rangle^2 l_c^2/2$, where l_c is the correlation length associated with the diffusion process and is given by the Einstein expression $l_c^2 = 2D_0\tau_c$, where D_0 is the free diffusion coefficient.

With this as background, we consider SDR's potential to probe the average background gradient $\langle G\rangle$ felt by the spins, when these are in the free diffusion regime. In this restrictionless $\tau_c \gg TE$ limit, the relevant time scales x, y associated with the SDR pulse sequence are shorter than τ_c, and one can probe the background gradient without knowledge of the correlation or restriction length l_c. Indeed, since the longest delay between pulses $\max\{x, y\} \ll \tau_c$, the peaks of the filter function $F(\omega, TE)$ introduced in Eq. (1), will appear at frequencies $\omega \gg 1/\tau_c$.[48,49,51] The decoherence time of the spin signal at the end of the SDR sequence is thus dominated by the "tail" of the spectral density $S(\omega) \sim \frac{\Delta\omega_{SE}^2}{\omega^2\tau_c\pi} = \frac{2\gamma^2\langle G\rangle^2 D_0}{\pi\omega^2}$ (dashed red line in Fig. 2).[49,53] To quantify this feature we consider the magnetization decays for the two parts of the SDR sequence in Fig. 1. The signal decay for the CPMG portion of the sequence ($x = y$ in Fig. 1) is well known,[42] and is given by

$$M_{CPMG}^{free}((N-1)x, N-1) = \exp\left\{-\frac{1}{12}\frac{\Delta\omega_{SE}^2}{\tau_c}(N-1)x^3\right\} = \exp\left\{-\frac{1}{12}\gamma^2\langle G\rangle^2 D_0(N-1)x^3\right\}. \quad (2)$$

As expected, M_{CPMG}^{free} is independent of τ_c. The decay for a Hahn sequence ($N = 1$ and $x = 0$ in Fig. 1) follows from setting $N - 1 = 1$ in this expression:

$$M_{Hahn}^{free}(y) = \exp\left\{-\frac{1}{12}\gamma^2\langle G\rangle^2 D_0 y^3\right\}. \quad (3)$$

Notice that, without pulses, the evolution of the free induction decay (FID) is

$$M_{FID}^{free}(TE) = \exp\left\{-\frac{1}{2}\Delta\omega_{SE}^2 TE^2\right\} \quad (4)$$

$$= \exp\left\{-\frac{1}{2}\gamma^2\langle G\rangle^2 D_0\tau_c TE^2\right\}. \quad (5)$$

Contrary to M_{CPMG}^{free} and M_{Hahn}^{free}, this expression depends on τ_c and consequently on the sample size.

While CPMG decays monitored as a function of x are normally used for measuring the diffusion coefficient, they can be also used for determining $\langle G\rangle$ when the diffusion coefficient is known. Figure 3 shows the features that will in such instances arise, if attempting to measure internal fields gradients $\langle G\rangle$ in the presence of global ΔB_0 inhomogenities. While the span of the external magnetic field ΔB_0 over the complete sample of length L is larger than the internal fields, this will not be the case for the external field changes Δb_0 if smaller distances Δr are considered. This lies at the heart of using CPMG, in combination with diffusion, to characterize $\langle G\rangle$ while avoiding ΔB_0's dominance. By relying on diffusion-driven fluctuations but refocusing the spins' coherent evolution before they have traveled long distances Δr, the $\langle\frac{\Delta B_0}{L}\rangle \approx \langle\frac{\Delta b_0}{\Delta r}\rangle \ll \langle G\rangle$ condition can be fulfilled. In these cases, the internal gradients that arise from microstructure-induced susceptibility effects, will dominate their global counterparts.

While this justifies the use of CPMG to monitor internal gradients, these arguments consider the spins' precession frequency fluctuations (as a function of TE) as the only source of

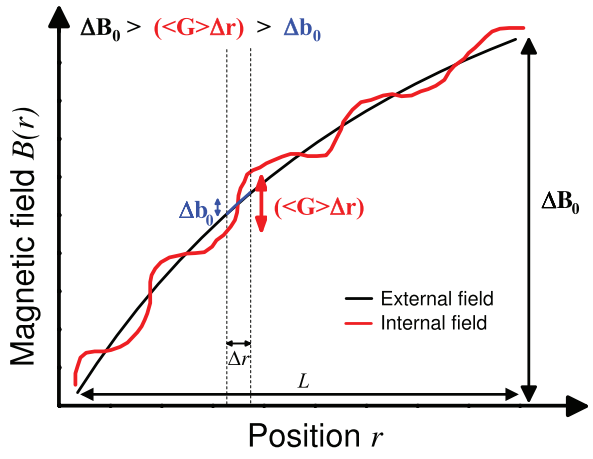

FIG. 3. Different sources and scales of magnetic field inhomogenities. The solid black line represents a global external variation over the full length L, carrying no morphological content. The red solid line shows the magnetic field additions generated by the susceptibility changes of interest. The global external ΔB_0 dominates the internal $\langle G\rangle\Delta r$; but dynamical decoupling allows one to choose times over which distances Δr are allowed to be explored by diffusion. On these length scales, the internal magnetic field gradients $\langle G\rangle$ are larger than the ones generated by the external magnetic field inhomogenity $\Delta b_0/\Delta r \approx \Delta B_0/L$.

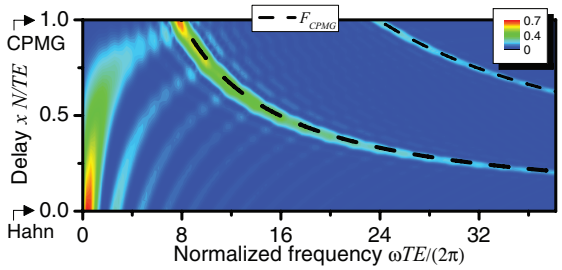

FIG. 4. Generic filter function $F(\omega, TE)$ of the SDR sequence, shown as normalized intensity for $N = 16$ and illustrating how different spectral modes can be probe by changing the delay x. The Hahn filter contribution dominates for $x = 0$ and the CPMG harmonics dominates for $x = TE/N$. The dashed line shows the behavior of the CPMG filter component.

decay. This will be valid if the applied pulses are ideal and if no other sources of decoherence exist; in reality, CPMG signals will also decay due to the pulses' non-idealities, and due to intrinsic spin-spin relaxation (T_2). The manner by which these decohering sources modify typical $S(\omega)$ spectral densities is shown by Fig. 2's empty circles. Such contributions can eclipse the power law tail of the diffusion spectrum, and are thereby known to limit the precision with which the sought parameters can be determined. In other words: since by measuring the $\langle G\rangle$-induced CPMG decay according to Eq. (2) one needs to vary TE/N by either keeping TE fixed and changing the number of pulses, or by keeping constant the number of pulses and changing TE, the diffusion-driven decay will be either contaminated by N-dependent contributions from the pulse imperfections, or it will reflect additional T_2 signal weightings.

To avoid these alternative sources of decoherence, the SDR sequence departs from the CPMG scheme by keeping fixed both the number of pulses N and the overall evolution time TE, and introducing non-equidistant delays into the sequence.[35,36] By systematically varying the ratio x/y one can still probe the power law tail of the spectral density $S(\omega)$ and determine $\langle G\rangle^2 D_0$, yet avoid the losses associated with changing TE or suffering from pulse-driven imperfections. The consequences of this choice follow from the formalism given in Eq. (1): the variable at the experimentalist's control in the SDR sequence is the filter function $F(\omega, TE)$, shown for a generic case in Fig. 4. This figure evidences how the Hahn and the CPMG contributions in $F(\omega, TE)$, will probe different modes of $S(\omega)$ as a function of x.[36,49]

Note that the fact that TE and N are constant means that T_2- or pulse-error-induced effects just rescale the overall spin magnetization, independent of x; no decoherence sources other than those related to diffusion need to be considered in SDR.

The formalism in Eq. (1) allows one to calculate an analytical solution for the SDR signal decay, as

$$\begin{aligned} &M_{SDR}(TE, x, y, N) \\ &\quad = M_{CPMG}((N-1)x, N-1) \\ &\qquad \times M_{\text{Hahn}}(y) \times M_{Cross-SDR}(TE, x, y, N), \end{aligned} \tag{6}$$

reflecting a Hahn-decay, a CPMG-decay, and a potential cross-term between the two filters that in principle cannot be neglected. A rigorous derivation of these various components is given in Ref. 36. While under restricted diffusion the cross-term in Eq. (6) is essential for endowing SDR with its high sensitivity for determining restriction lengths,[36] the Appendix demonstrates why, for the free diffusion regime here considered, this cross term contribution $M_{Cross-SDR}$ is negligible. Therefore, the signal decay for SDR in this latter case is given by

$$\begin{aligned} &M_{SDR}^{free-diff}(TE, x, y, N) \\ &\quad = M_{CPMG}((N-1)x, N-1) \times M_{\text{Hahn}}(y) \\ &\quad = \exp\left\{-\frac{1}{12}\gamma^2 \langle G\rangle^2 D_0[(N-1)x^3 + y^3]\right\}. \end{aligned} \tag{7}$$

Considering that $(N-1)x + y = TE$ and using dimensionless variables normalized by an equidistant delay TE/N, i.e., $x' = xN/TE$ and $y' = yN/TE$, the SDR decay can be expressed solely as a function of the x' variable

$$\begin{aligned} &M_{SDR}^{free-diff}(TE, x', N) \\ &\quad = \exp\left\{-\frac{1}{12}\gamma^2 \langle G\rangle^2 D_0 TE^3 \right. \\ &\qquad \times \left[1 - 3\frac{N(N-1)}{N^2}x' + 3\frac{(N^2 - 2N + 1)}{N^2}x'^2 \right. \\ &\qquad \left.\left. - \frac{(N^2 - 3N + 2)}{N^2}x'^3\right]\right\}. \end{aligned} \tag{8}$$

The amplitude modulation of this method is then given by the difference between the Hahn-echo extreme $M_{SDR}^{free-diff}(TE, x' = 0, N) = M_{Hahn}^{free-diff}(TE)$, and the CPMG extreme $M_{SDR}^{free-diff}(TE, x' = 1, N) = M_{CPMG}^{free-diff}(TE, N)$. Figure 5 shows typical SDR curves following from Eq. (8) as a function of x' and y, for $TE = 80$ ms, $D_0 = 2.01 \times 10^{-5}$ cm^2/s, $\langle G\rangle = 1$G/cm and different values of N. Notice that all curves converge towards $x' = 0$ to the Hahn decay $M_{Hahn}^{free-diff}(TE)$, and for $x' = 1$ to the CPMG decay $M_{CPMG}^{free-diff}(TE, N)$ shown by the empty circles. Note as well that by increasing N, the SDR modulations converge to the Hahn modulation for a refocusing period y, i.e., to $M_{Hahn}^{free-diff}(y)$ (Fig. 5(b)). Important to stress is the amplitude modulation that all SDR curves undergo as a function of x'. This amplitude modulation $\Delta M_{SDR} = M_{CPMG}^{free-diff}(TE, N) - M_{Hahn}^{free-diff}(TE)$ depends on $\langle G\rangle^2 D_0$ and on the chosen TE, N. If a reasonable value for D_0 is assumed, these modulations can thus map the background gradients $\langle G\rangle$. Alternatively, by measuring in a separate experiment the fluid's D_0, fitting SDR's modulation will yield a quantitative description of the background gradients in a constant-time, constant-pulsing fashion. Suitable experiments to extract D_0 values may rely on oscillating-gradient or CPMG sequences;[51,54] alternatively, Non-uniform Oscillating-Gradient Spin-Echo (NOGSE)

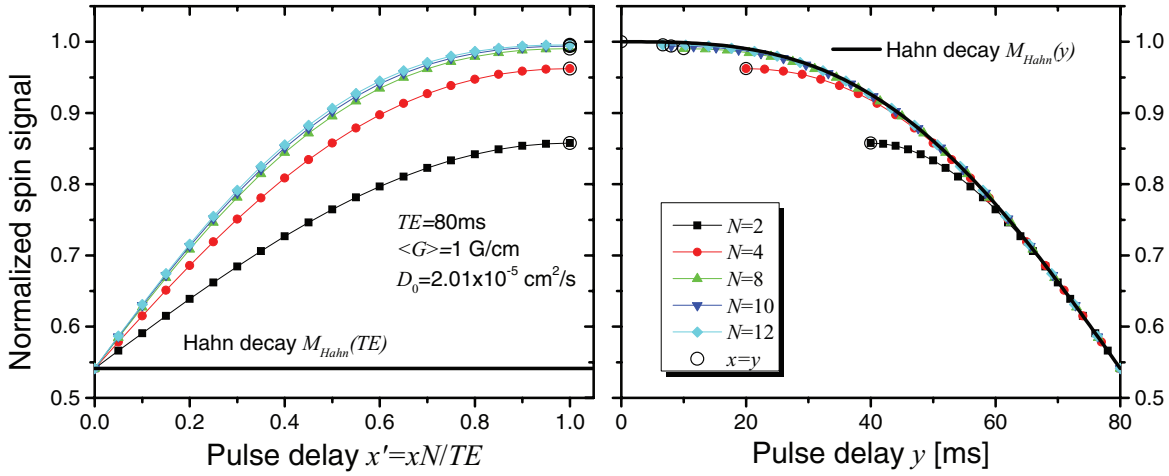

FIG. 5. SDR modulations as a function of $x' = xN/TE$ (left) and y (right) for different number of pulses N, and for the indicated D_0, TE, and $\langle G \rangle$ values. The thick solid line gives the Hahn decay (i.e., a simple Hahn spin echo sequence with a total evolution time of TE) in the left panel, while in the right panel it is for a total evolution time y. The empty circles show the CPMG value for the SDR modulations.

sequences[37] incorporating strong external applied gradients would also deliver this information.

III. EXPERIMENTAL SETUP

SDR's abilities to monitor background gradients were experimentally tested on a 9.4 T Bruker Avance NMR spectrometer operating at 400.17 MHz for ^{1}H's, equipped with a Micro5 imaging probe capable of producing maximum pulsed-field-gradients of 291 G/cm in all three dimensions. To explore the usefulness of this diffusion-based approach, a series of NMR imaging experiments were carried out. These experiments were performed in *ex vivo* mouse brains, and were aimed at characterizing the internal background gradients' spatial distribution. The MRI sequence shown in Fig. 6 was used; this begins with a slice-selective excitation, follows with a SDR "module" including N slice-selective refocusing pulses, and concludes with a conventional 2D line-by-line image encoding scheme. The formaline-fixed mouse brains analyzed were washed twice with PBS, left thereafter in PBS overnight, dried externally, and placed in a 10 mm NMR tube for their examination in the magnet. Brains were aligned with their anterior–posterior axes coinciding with the z-direction, and allowed to thermally equilibrate for ∼2 h prior to the MRI experiments.

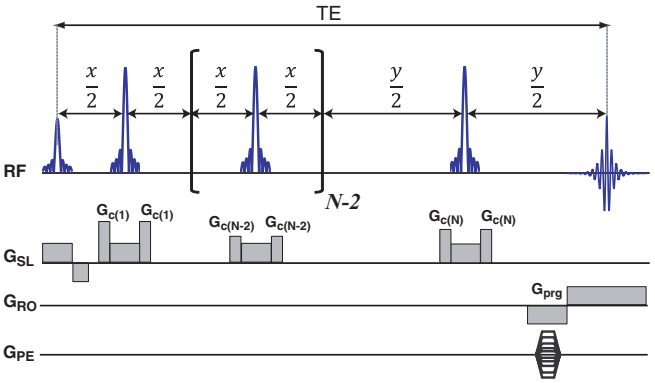

FIG. 6. SDR MRI sequence assayed, involving a slice-selective (SL) excitation, followed by a train of slice-selective SDR refocusing π-pulses surrounded by unequal gradient crushers G_c, and concluded with phase encoding (PE), purging (prg), and readout (RO) gradients to encode a two-dimensional image. The notation $G_{c(i)}$ denotes pairs of crushers associated with the ith SDR pulse; these crusher pairs must be applied randomly both in magnitude and orientation to avoid refocusing of unwanted coherence pathways. In our implementation, the following imaging parameters were used: TE = 80 ms, repetition time = 3.5 s, number of dummy scans = 4, number of averages = 8, slice thickness – 500 μm, field of view – 11 × 11 (mm)^2 with a matrix size = 96 × 96 leading to an isotropic in-plane resolution of 114 × 114 (μm)^2. SDR-related parameters were: N = 4; x was varied from 3 to 20 ms in 10 steps, whereas y was concomitantly reduced from 71 ms to 20 ms. The gradients associated with the slice-selective pulses contribute a diffusion-driven decay that is an order of magnitude smaller than that arising from the internal gradients.

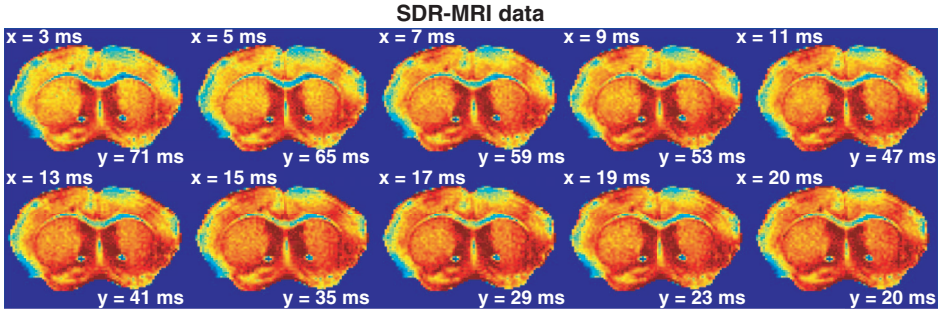

FIG. 7. Raw SDR MRI images arising from *ex vivo* mouse brain experiments acquired with the sequence and parameters shown in Fig. 6 for the indicated x- and y-combinations. Signal increases with increasing x-values are clearly evident in these raw data.

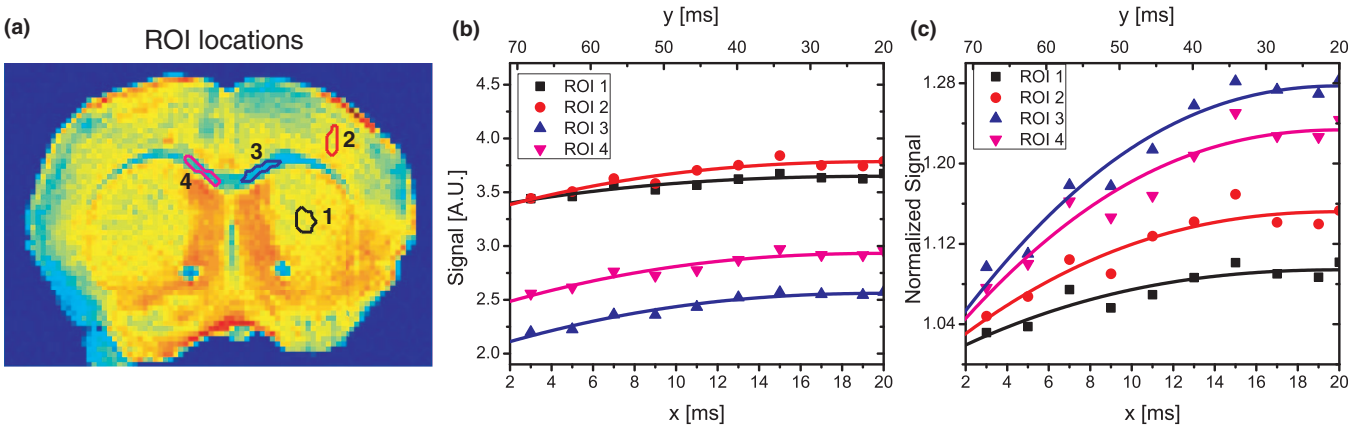

FIG. 8. Region-of-interest (ROI) analysis of SDR MRI data. (a) ROI definitions within the MRI image. (b) Absolute-valued SDR MRI signal evolution in each ROI (symbols) along with fittings of the experimental points to Eq. (8) with only $\langle G\rangle^2 D_0$ and the overall signal amplitude as fitting parameters. (c) Normalized SDR MRI signal evolution. Note the good agreement between experimental data and theory, and the differential increases in the SDR MRI signals with increasing x-values. The contrast in (c), manifested as the difference between the two extremes of the SDR curve, reflects the magnitude of the $\langle G\rangle^2 D_0$ term.

IV. SDR-BASED DIFFUSION MRI: MAPPING BACKGROUND GRADIENTS IN BIOLOGICAL TISSUES

Figure 7 shows representative raw data obtained from SDR MRI scans in a mouse brain. Note the clear signal changes observed with changing x-values, with most brain regions showing the expected increase in signal as the x interval is prolonged. To further analyze this SDR evolution, a number of regions of interest (ROIs) were defined within representative grey matter (Fig. 8(a), black and red ROIs) and white matter tissues (Fig. 8(a), blue and magenta ROIs). The averaged signal in each of these ROIs was then plotted (Fig. 8(b), symbols). A signal increase was clearly observed in all of these ROIs, as expected from the theory outlined above. Upon fitting the data arising from these ROIs to Eq. (8) (Fig. 8(b), solid lines) with only $\langle G\rangle^2 D_0$ as a fitting parameter, we found that all of these ROIs followed the predicted SDR evolutions, with a very good agreement between the experimental data and fitted curves. Another view of these data is given in Fig. 8(c), showing the signal normalized to the first SDR point $M_{SDR}^{free}(TE, x = 0, N)$ of the fitted curve, and revealing that the range of signal variation was $\sim 5\% - 30\%$ of the initial signal. These relative signal changes, when viewed in such normalized scale, directly contrast $\langle G\rangle^2 D_0$ for each ROI.

The SDR MRI data were then subject to a pixel-by-pixel fitting of the data to Eq. (8), with only $\langle G\rangle^2 D_0$ and the overall signal amplitude as fitting parameters. $\langle G\rangle$ maps can then be obtained from the $\langle G\rangle^2 D_0$ extracted for each pixel, if D_0 is known or has been measured by a separate experiment (cf. Sec. II). Figure 9 assumes that D_0 was uniform throughout the entire brain and equal to 0.7×10^{-5} cm^2/s[55,56] related measurements (not shown) suggested that little variation in D_0 occurs within the brain. The contrast derived from this SDR map is dramatically different from any of the raw MRI images, reflecting the new information extracted from these data. The magnitudes of these background brain gradients range from $\sim$0.05 to $\sim$0.9 G/cm; remarkably, this $\langle G\rangle$-based contrast in the brain appears spontaneously symmetric, suggesting that it arises due to purely internal effects and confirming SDR's independence from global shimming-induced field distributions. Interestingly white matter tissue, and specifically the corpus callosum, evidences stronger background gradients, consistent with recent literature suggesting larger susceptibility-induced field distributions in these regions.[15,57] The molecular origins of these contrasts are under investigation but it seems that myelin, a major constituent of white matter, may be at least in part responsible.[16] It should be added that the magnitudes of the internal gradients in Fig. 9 appear to be slightly larger than would be expected for soft tissues; this may be due in part to our D_0 value assumption, or due to decays introduced by crusher gradients during the sequence. Changes on the former's value or accounting for the latter would rescale the internal gradient map, but would leave unchanged its overall

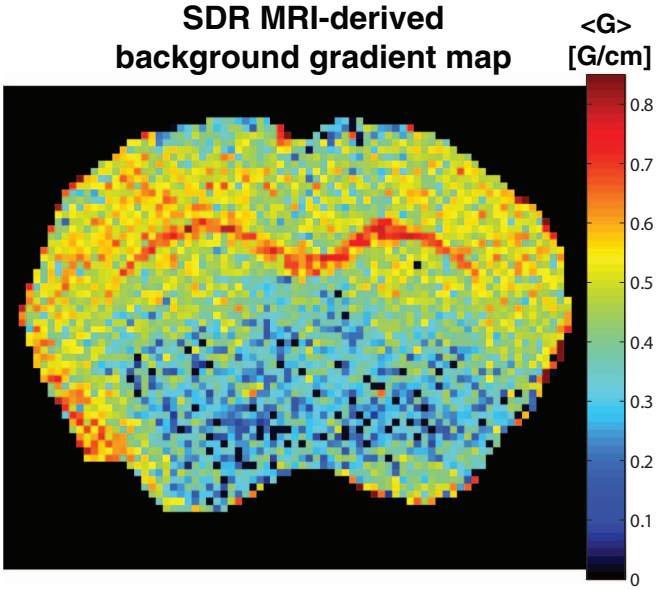

FIG. 9. Background gradient $\langle G\rangle$ map derived from the SDR MRI data. The map arises from a pixel-by-pixel fitting of the data in Fig. 7, of the kind that was illustrated in Fig. 8 for four ROIs, assuming that D_0 is identical throughout all ROIs.

morphology. This reflects the self-normalized nature being fit in these SDR signal measurements.

V. CONCLUSIONS

This study introduced a new method for determining internal gradients induced by susceptibility effects in structured samples. By probing the decay dynamics within a regime where spins diffuse effectively freely, we were able to extract unknown background gradient strengths, from simple analytical fits; the sole unknown to extract these maps was the free diffusion coefficient D_0, which can usually be reasonably assumed or determined by separate experiments with known applied gradients. The method is based on applying a non-equidistant spin-echo sequence that selectively modulates diffusion decoherence effects, while keeping fixed the total evolution time and the number of pulses.[36] By changing the pulse delay distribution, the ensuing SDR sequence only probes the spectral density of the spin's frequency fluctuations due to the diffusion process. Analytical solutions of the diffusion-driven modulations based on a spectral density approach, led to the background gradient maps being sought. As a test of this method, we applied it to generate a new source of MRI contrast based on the internal gradient strengths in a mouse's brain. Compared to other approaches utilizing diffusion decay for probing the internal gradients,[3,19,20,31–33] the SDR approach offers a constant-time and constant-pulsing mode of operation which alleviates decoherence effects related to T_1, T_2, or RF imperfections, albeit at the expenses of a relatively long TE (which might bias the measurement towards longer T_2 species). This approach to $\langle G \rangle$-mapping is by contrast to most contemporary methods that aim at detecting susceptibility-induced effects, by either mapping the phase of gradient-echo images[11] or by weighting the signals by T_2^* effects.[14] Such methods are more susceptible than SDR to dephasing due to static (B_0-based) inhomogenities, which may obscure the desired microstructural information. This may be further exacerbated by phase-unwrapping inaccuracies[58] or signal distortions near interfaces. SDR MRI on the other hand is much less prone to static inhomogenities due to its application of refocusing π-pulses, rendering the methodology sensitive only to diffusion-assisted decoherence. Finally, it is worth remarking that in every given pixel of a SDR image the underlying structures will induce a distribution of internal gradients, both in magnitude[29] and possibly also in orientations.[30] $\langle G \rangle$ maps like the ones shown in Fig. 9 only reflect an averaged value across this distribution; one could envision that, by applying alternative SDR gradient strategies, also these distributions might be directly probed. Work along such lines of thought is currently in progress.

ACKNOWLEDGMENTS

We are grateful to Pieter Smith, Guy Bensky, and Gershon Kurizki (Weizmann Institute) for fruitful discussions. This research was supported by the Israel Science Foundation through Grant No. ISF-1142/13, a Helen and Martin Kimmel Award for Innovative Investigation, and the generosity of the Perlman Family Foundation. G.A.A. acknowledges the support of the European Commission under the Marie Curie Intra-European Fellowship for career Development Grant No. PIEF-GA-2012-328605. N.S. acknowledges the Weizmann Institute for a Dean Fellowship.

APPENDIX: ANALYTICAL EXPRESSIONS AND JUSTIFICATION OF NEGLECTING SDR'S HAHN-CPMG CROSS-TERM UNDER FREE DIFFUSION

The full analytical expression and justification of Eq. (6) can be found in Ref. 36. We justify here our neglecting of the $M_{Cross-SDR}(TE, x, y, N)$ cross-term on the SDR modulations, on the basis of a Taylor expansion of those expressions as a function of TE/τ_c – a reasonable assumption since the free diffusion regime fulfills $TE/\tau_c \ll 1$. The cross-term in question is then different depending on whether the number of pulses N is even or odd

$$\ln\left\{M^{even-N}_{Cross-SDR}(TE, x, y, N)\right\} \approx \frac{1}{16}\gamma^2 \langle G\rangle^2 D_0 TE^3 \left\{\left(\frac{TE}{\tau_c}\right)\left[\frac{(N-1)^2 x'^4}{N^4} - 2\frac{(N-1)x'^3}{N^3} + \frac{x'^2}{N^2}\right] + \mathcal{O}\left(\left(\frac{TE}{\tau_c}\right)^2\right)\right\} \quad \text{(A1)}$$

and

$$\ln\left\{M^{odd-N}_{Cross-SDR}(TE, x, y, N)\right\} \approx \frac{1}{32}\frac{\Delta\omega^2_{SE}}{\tau_c} TE^3 \left\{\left(\frac{TE}{\tau_c}\right)^2\left[\frac{(N-1)^3 x'^5}{N^5} - 2\frac{(N-1)^2 x'^4}{N^4} + \frac{(N-1)x'^3}{N^3}\right] + \mathcal{O}\left(\left(\frac{TE}{\tau_c}\right)^3\right)\right\}, \quad \text{(A2)}$$

where $x' = xN/TE$. These two expressions show that cross-terms are scaled by $(\frac{TE}{\tau_c})$ and $(\frac{TE}{\tau_c})^2$ terms for N even or odd, respectively. These are both smaller than the unity scaling appearing in both the Hahn- and CPMG-modulations given in Eq. (8), thereby justifying their neglect. Physically, this neglect reflects the fact that the Hahn and CPMG-derived filter functions are very narrow compared with the changes of $S(\omega)$, and while the direct terms are strictly positive, the cross terms are fast oscillatory functions around zero that cancel out.

[1] P. T. Callaghan, *Principles of Nuclear Magnetic Resonance Microscopy* (Oxford University Press, 1993).
[2] P. Sen and S. Axelrod, J. Appl. Phys. **86**, 4548 (1999).
[3] J. Kuntz, G. Trausch, P. Palmas, P. Mutzenhardt, and D. Canet, J. Chem. Phys. **126**, 134904 (2007).
[4] A. Pathak, B. Ward, and K. Schmainda, Neuroimage **40**, 1130 (2008).
[5] Y. Cheng, J. Neelavalli, and E. Haacke, Phys. Med. Biol. **54**, 1169 (2009).
[6] J. Mitchell, T. Chandrasekera, and L. Gladden, J. Chem. Phys. **132**, 244705 (2010).
[7] J. Lee, K. Shmueli, M. Fukunaga, P. van Gelderen, H. Merkle, A. Silva, and J. Duyn, Proc. Natl. Acad. Sci. U.S.A. **107**, 5130 (2010).
[8] E. Haacke, Y. Xu, Y. Cheng, and J. Reichenbach, Magn. Reson. Med. **52**, 612 (2004).
[9] L. de Rochefort, T. Liu, B. Kressler, J. Liu, P. Spincemaille, V. Lebon, J. Wu, and Y. Wang, Magn. Reson. Med. **63**, 194 (2010).
[10] S. Ogawa, T. Lee, A. Nayak, and P. Glynn, Magn. Reson. Med. **14**, 68 (1990).

[11]C. Liu, Magn. Reson. Med. **63**, 1471 (2010).
[12]C. Liu, W. Li, B. Wu, Y. Jiang, and G. Johnson, Neuroimage **59**, 1290 (2012).
[13]C. Liu and W. Li, Neuroimage **67**, 193 (2013).
[14]J. Lee, P. van Gelderen, L. Kuo, H. Merkle, A. Silva, and J. Duyn, Neuroimage **57**, 225 (2011).
[15]S. Oh, Y. Kim, Z. Cho, and J. Lee, Neuroimage **73**, 71 (2013).
[16]W. Li, B. Wu, A. Avram, and C. Liu, Neuroimage **59**, 2088 (2012).
[17]W. Chen, S. Foxley, and K. Miller, Neuroimage **70**, 1 (2013).
[18]G. Zheng and W. Price, Concepts Magn. Reson. **30A**, 261 (2007).
[19]B. Sun and K.-J. Dunn, Phys. Rev. E **65**, 051309 (2002).
[20]H. Cho, E. Sigmund, and Y. Song, Materials **5**, 590 (2012).
[21]R. Karlicek, Jr. and I. Lowe, J. Magn. Reson. **37**, 75 (1980).
[22]M. I. Hrovat and C. G. Wade, J. Magn. Reson. **44**, 62 (1981).
[23]M. I. Hrovat and C. G. Wade, J. Magn. Reson. **45**, 67 (1981).
[24]R. M. Cotts, M. J. R. Hoch, T. Sun, and J. T. Markert, J. Magn. Reson. **83**, 252 (1989).
[25]P. Z. Sun, J. G. Seland, and D. Cory, J. Magn. Reson. **161**, 168 (2003).
[26]J. Finsterbusch, J. Magn. Reson. **191**, 282 (2008).
[27]A. Bar-Shir and Y. Cohen, Magn. Reson. Imaging **26**, 801 (2008).
[28]N. Shemesh, E. Ozarslan, T. Adiri, P. Basser, and Y. Cohen, J. Chem. Phys. **133**, 044705 (2010).
[29]H. Cho, S. Ryu, J. Ackerman, and Y. Song, J. Magn. Reson. **198**, 88 (2009).
[30]S. Han, Y. Song, F. Cho, S. Ryu, G. Cho, Y. Song, and H. Cho, J. Magn. Reson. **212**, 386 (2011).
[31]Y.-Q. Song, S. Ryu, and P. N. Sen, Nature (London) **406**, 178 (2000).
[32]Y. Song, J. Magn. Reson. **143**, 397 (2000).
[33]Q. Chen, M. Gingras, and B. Balcom, J. Chem. Phys. **119**, 9609 (2003).
[34]P. Sen, A. Andre, and S. Axelrod, J. Chem. Phys. **111**, 6548 (1999).
[35]P. E. S. Smith, G. Bensky, G. A. Álvarez, G. Kurizki, and L. Frydman, Proc. Natl. Acad. Sci. U.S.A. **109**, 5958 (2012).
[36]G. A. Álvarez, N. Shemesh, and L. Frydman, Phys. Rev. Lett. **111**, 080404 (2013).
[37]N. Shemesh, G. A. Álvarez, and L. Frydman, J. Magn. Reson. **237**, 49–62 (2013).
[38]A. Abragam, *Principles of Nuclear Magnetism* (Oxford University Press, London, 1961).
[39]J. Stepisnik, Physica B **270**, 110 (1999).
[40]R. P. Kennan, J. Zhong, and J. C. Gore, Magn. Reson. Med. **31**, 9 (1994).
[41]E. Hahn, Phys. Rev. **80**, 580 (1950).
[42]H. Carr and E. Purcell, Phys. Rev. **94**, 630 (1954).
[43]S. Meiboom and D. Gill, Rev. Sci. Instrum. **29**, 688 (1958).
[44]J. Stepisnik, Physica B+C **104**, 350 (1981).
[45]P. T. Callaghan and J. Stepisnik, J. Magn. Reson. **117**, 118 (1995).
[46]A. G. Kofman and G. Kurizki, Phys. Rev. Lett. **87**, 270405 (2001).
[47]A. G. Kofman and G. Kurizki, Phys. Rev. Lett. **93**, 130406 (2004).
[48]A. Ajoy, G. A. Álvarez, and D. Suter, Phys. Rev. A **83**, 032303 (2011).
[49]G. A. Álvarez and D. Suter, Phys. Rev. Lett. **107**, 230501 (2011).
[50]J. R. Klauder and P. W. Anderson, Phys. Rev. **125**, 912 (1962).
[51]S. Lasic, J. Stepisnik, and A. Mohoric, J. Magn. Reson. **182**, 208 (2006).
[52]J. Stepisnik, S. Lasic, A. Mohoric, I. Sersa, and A. Sepe, J. Magn. Reson. **182**, 195 (2006).
[53]D. Pfitsch, A. McDowell, and M. S. Conradi, J. Magn. Reson. **139**, 364 (1999).
[54]E. C. Parsons, M. D. Does, and J. C. Gore, Magn. Reson. Imaging **21**, 279 (2003).
[55]M. D. Does, E. C. Parsons, and J. C. Gore, Magn. Reson. Med. **49**, 206 (2003).
[56]J. Xu, M. D. Does, and J. C. Gore, Magn. Reson. Med. **61**, 828 (2009).
[57]X. He and D. Yablonskiy, Proc. Natl. Acad. Sci. U.S.A. **106**, 13558 (2009).
[58]A. Rauscher, M. Barth, K.-H. Herrmann, S. Witoszynskyj, A. Deistung, and J. R. Reichenbach, Magn. Reson. Imaging **26**, 1145 (2008).